Modern Applied Science; Vol. 10, No. 4; 2016
ISSN 1913-1844 E-ISSN 1913-1852
Published by Canadian Center of Science and Education

ZnO QDs Deposited on Si by Sol-Gel Method: Role of Annealing Temperature on Structural and Optical Properties

Hayder J. Al-Asedy[1], Noriah Bidin[2], Khaldoon N. Abbas[1,3] & Mohammed A. Al-Azawi[1]

[1] Department of Physics, Faculty of Science, Universiti Teknologi Malaysia, Johor Bahru, Malaysia

[2] Advance Photonic Science Institute, Faculty of Science, Universiti Teknologi Malaysia, Johor Bahru, Malaysia

[3] Mustansiriya University, Faculty of Science, Physics Department, Baghdad, 00964, Iraq

Correspondence: Noriah Bidin, Advance Photonic Science Institute, Faculty of Science, Universiti Teknologi Malaysia, Johor Bahru, Johor, 81310, Malaysia. E-mail:noriah.utm@gmail.com

Received: October 24, 2015 Accepted: November 5, 2015 Online Published: January 13, 2016

doi:10.5539/mas.v10n4p12 URL: http://dx.doi.org/10.5539/mas.v10n4p12

Abstract

Zinc acetate, propanol, and ethanolamine are used to synthesize ZnO quantum dots (QDs) via the sol–gel method. Spin coating at 220°C is then employed to prepare ZnO thin films consist of QDs. The effects of thermal annealing temperature on the structural and optical properties of the samples are investigated. The prepared QDs are characterized using X-ray diffraction (XRD), field emission scanning electron microscopy (FESEM), and photoluminescence spectroscopy (PL). XRD patterns reveal the crystalline nature of samples existing in the hexagonal wurtzite phase. Increasing annealing temperatures bring about changes to the crystal orientation through the c-axis and increase the size of the QDs from ~10 nm to ~22 nm; this increment can be explained by a coarsening mechanism and the Ostwald ripening process. The observed broadening of X-ray peaks confirms the evolution of crystalline phases in the ZnO QDs. Quantitative analysis of size-dependent strain effects is performed through the Williamson-Hall model. The QD mean size estimated from FESEM and XRD displays high consistency. Room-temperature PL peaks of 3.37ev are attributed to the radiative recombination of electrons and holes from the ZnO QDs/Si interface.

Keywords: ZnO, sol–gel method, annealing temperature, structural & optical properties

1. Introduction

1.1 Introduction of the Problem

Zinc oxide (ZnO),an n-type metal oxide semiconductor with a wide band-gap(3.36 eV), has received considerable research attention because of its strong exciton binding energy of 60 meV at room temperature (Liu et al., 2013), large saturation velocity of 3.2×10^7 cm s^{-1}(Tekmen et al., 2013), and non-toxicity (Thomas et al., 2014). In general, ZnO exists as a hexagonal structure with c/a = 1.65. This form, however, may vary according to the growth conditions applied. Several synthesis methods, including sol–gel, hydrothermal, solvothermal, sonochemical, combustion, chemical vapor deposition (CVD), vapor-liquid solid (VLS), and pulsed laser deposition, have been developed over the years to control the growth of ZnO nanostructures (Kamalianfar et al., 2014; Zak et al., 2013; Razali et al., 2011; Yousefi et al., 2012; Yousefi et al., 2010; Zhanget al., 2004).Annealing is considered a promising route to tune the properties of ZnO nanostructure (Ashrafiet al., 2004; Radet al.,2013; Yousefi et al., 2013; Yousefi et al., 2013; Zak et al., 2012; Zak et al., 2012; Zamiri et al., 2013). The crystallite size and lattice parameters of a crystal system are greatly affected by the annealing temperature. The lattice strain and crystallite size are the two main factors leading to broadening of diffraction peaks. Lattice strain originates from lattice imperfections or dopants and alters peak intensities and positions (Ramgir et al., 2006). Uniform strains change peak positions, and non-uniform strains promote peak broadening.

In this study, we fabricate ZnO QDs on silicon substrates using a simple sol–gel method following by spin coating. The effects of annealing temperature on the crystalline structure and surface morphology of the samples are investigated in detail by X-ray diffraction (XRD), energy dispersive X-ray spectroscopy (EDX), and field emission scanning electron microscopy (FESEM). The results of this work may further establish the belief that by carefully controlling their process parameters, ZnO QDs may be utilized in spintronic applications. ZnO is used in several applications due to its high transparent and good electrical conductivity. Some of these applications are gas sensor and photovoltaic devices, water waste treatment, photo catalysis, chemical

remediation, photo-initiazation of polymerization reactions, quantum dot devices, and solar energy conversion.

1.2 Experimental Details

The ZnO films are deposited by a sol–gel process using a spin coating method onto p-Si (100) substrates.Firstly, the $NH_4OH+H_2O_2$+6 deionized (DI) should be boiled for 10 min with (18 MΩ- DI) water. Then before forming a ZnO layer on p-Si substrate, the native oxide on the polish surface of the substrate is removed from HF: H_2O (1:10) solution. Finally, the wafer is rinsed in DI water at last dried by N_2 gas.

The zinc precursor solution is prepared by dissolving zinc acetate dihydrate (ZnAc; the starting material) in 2-propanol (the solvent) to obtain a final concentration of 0.1 M. Ethanolamine (EA; the stabilizer) is added to this mixture to obtain a stable and transparent solution. The molar ratio of ZnAc to EA is maintained at 1:1. The sol is stirred at 60 °C until a transparent and homogeneous solution is obtained.

The sol is allowed to drip onto the center of the substrate, which is immediately spun at 3000 rpm for 20 s. After each coating, the films are dried at 220°C for 10 min. The coating–drying cycles are repeated 10times, and the films are annealed at 425, 450, 475, or 500°C for 2h in ambient atmosphere of the samples are characterized by XRD (Bruker D8 Advance diffractometer) with Cu-K$\alpha_1$radiation(1.5406 A°) at 40 kV and 100 mA over the 2θrange of 25°–75°. A scanning speed of ~ 1.2°/min and a resolution of 0.011°are also employed. The elemental compositions of the samples are analyzed by an EDX diffractometer attached to a FESEM instrument (ZEISS SUPRA).

2. Results and Discussion

Figure 1 illustrates the XRD patterns ofZnO QDs annealed at 425–500 °C. The peaks detected are indexed to the hexagonal structure of ZnO and conform to those described in PDF No. 00-036-1451. The intensity of all diffraction peaks increases with increasing annealing temperature. This increment is ascribed to the impacts of disorders or defects removed by the annealing process; removal of these defects decreases the strain and improves add atom mobility, thereby enhancing the crystallization quality of ZnO by providing an abundant supply of thermal energy (Mandal et al., 2008).

The lattice parameters are calculated by (Gondal et al., 2009):

$$a = \frac{\lambda}{\sqrt{3}\sin\theta_{100}} \quad , c = \frac{\lambda}{\sin\theta_{002}} \tag{1}$$

The planer distance is determined by Bragg equation as follows:

$$n\lambda = 2d\sin\theta$$

Where *d* is the distance between two planes with lattice geometry

The hexagonal structure volume is calculated by (Cullity,1956):

$$V = \frac{\sqrt{3}a^2c}{2} = 0.866a^2c \tag{2}$$

Equations 1 and 2 are used to calculate the lattice constant values (a &c) and volume which are given in table1.

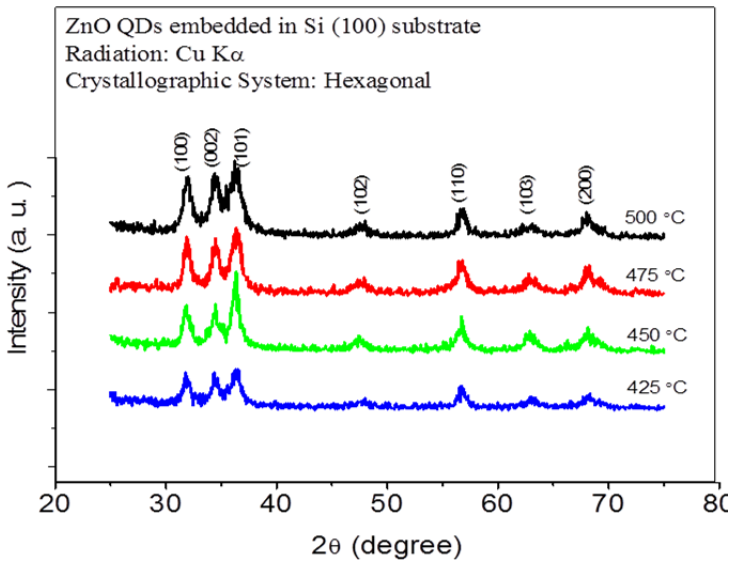

Figure 1. XRD pattern of the ZnO QDs deposited at different annealing temperatures

The Zn–O bond length L in the wurtzite structure can be estimated from the expression (3) (Yakuphanoglu F et al., 2007, p.2180) which are given bellow:

$$L=\sqrt{(\frac{a^2}{3}+(\frac{1}{2}-u)^2c^2)},\ u=\frac{a^2}{3c^2}+0.25 \quad (3)$$

The texture coefficient (TC) reflects the texture of a particular plane and indicates the preferred growth orientation of a crystal; this coefficient is defined as (Barret &Massalski, 1980):

$$TC\ (hkl)\ =\frac{I(hkl)/I_{\circ}(hkl)}{\sum nI(hkl)/I_{\circ}(hkl)}\ \ X100\ \ \% \quad (4)$$

Where TC (hkl) is the texture coefficient of the (hkl) plane, n is the number of reflections, and I (hkl) and I° (hkl) are the measured and relative intensities of the corresponding plane given in JCPDS Card No. 36-1451, respectively. Variations in TC among the peaks of the wurzite lattice are shown in Table 1. The highest TC occurs in the (101) plane.

Table 1. The variation of TC peak patterns of the wurzite lattice

Annealing Temperature	2θ ±0.01	hkl	d_{hkl}(nm)±0.0005	Lattice parameter (Å) ± 0.0005	V(nm^3)±0.0002	TC/ (%)	*FWHM (rad)*
425	31.854	100	2.8070	a=3.2273	0.0476	0.2688	0.608
	34.453	002	2.6010			0.2621	0.456
	36.348	101	2.4696	c=5.2086		0.3069	0.869
	56.802	102	1.6195			0.1620	0.555
450	31.995	100	31.995	a=3.2413 c=5.2020	0.0474	0.2715	0.493
	34.408	002	34.408			0.2847	0.554
	36.546	101	36.546			0.3078	0.510
	56.847	102	56.847			0.1357	0.451
475	31.895	100	31.895	a=3.2412 c=5.1741	0.0478	0.2773	0.478
	34.644	002	34.644			0.2802	0.485
	36.550	101	36.550			0.3155	0.686
	56.890	102	56.890			0.1284	0.590
500	31.840	100	2.8082	a=3.2427 c=5.1966	0.0476	0.2240	0.545
	34.490	002	2.5983			0.2278	0.430
	36.341	101	2.4701			0.3733	0.448
	56.709	102	1.6219			0.1708	0.390

The dislocation density (Table 2), which represents the number of defects in the film, is determined from the following equation. Dislocation densities exhibit a marked reduction with increasing annealing temperature, indicating a lower concentration of lattice imperfections (Ergin et al., 2009).

$$\delta = \frac{n}{D^2} \tag{5}$$

Where n is a factor that equals unity at the minimum dislocation density and D is the grain size. The values of strain along the c-axis (ε_{zz}) are determined by using the following formula (Ghosh et al., 2004):

$$\varepsilon_{zz} = \frac{c - c_\circ}{c_\circ} \text{ x100} \tag{6}$$

Where c_0 is equal to 5.20661 A° which is the lattice parameter of the strained ZnO films obtained from unstrained lattice parameter of ZnO that extracted from X-ray diffraction data (JCPDS 36-1451). The strain value can be negative (compressive) or positive (tensile). As can be seen from Table 1 the heat-treated process gives smaller c values than the ZnO powder. Zhang et al., have also reported slightly smaller c values for nanocrystalline ZnO thin films prepared on p-type Si(1 0 0) substrates by a sol–gel method followed by heat-treatment (Zhang et al., 2006). ZnO QDs have a number of defects such as oxygen vacancies, lattice disorders, etc. As a result of annealing, these defects are removed and the lattice contracted. Also lattice relaxation due to dangling bonds should be considered. The dangling bonds on ZnO surface interact with oxygen ions from the atmosphere and due to electrostatic attraction, lattice is slightly contracted.

For hexagonal lattice, the stress (σ_{film}) parallel to film surface can be obtained from equation (7) (Shahzad et. al., 2013):

$$\sigma_{film} = [2C_{13}^2 - C_{33}(C_{11} + C_{12})/2C_{13}] \times \varepsilon \tag{7}$$

The elastic stiffness constants C_{ij} for single crystal wurtzite ZnO are C_{11} = 208.8 GPa, C_{12} = 119.7 GPa, C_{13} = 104.2 GPa, and C_{33} = 213.8 GPa. The relevant ε_{zz} and σ_{film} are listed in Table 2.

Table 2. Annealing temperature dependent QDs sizes, density of dislocation**,** strain and stress

Annealing Temperature (°C)	Scherrer Estimate	Estimate from W-H Plot			Densityof Dislocation	ε_{zz} (%)	σ_{film} (GPa)
	D(nm)	D(nm)	$\varepsilon \times 10^{-3}$	FESEM	$x10^{-5}$ (nm^{-2})		
425	9	10	4.90	10	1234.56	0.03822	- 8.8980
450	12	14	2.83	14	694.444	- 0.08854	20.6130
475	16	15	2.83	20	390.625	- 0.62439	145.364
500	17	20	1.92	22	346.021	- 0.19225	44.7579

Strain obviously decreases with increasing annealing temperature, because the small amount of intrinsic stress is presented which normally arise from expansion of film volume during increasing of annealing temperatures. The negative sign of ε_{zz} belongs to thermal stress.

The XRD peak broadening analysis is used to evaluate the nanocrystallite size. The sizes are estimated from Scherrer equation= $K\lambda/\beta \cos\theta$.

where D is the crystallite size, λ is the wavelength of the radiation (1.5406 Å for Cu–K_α radiation), K is a constant with a value of about 0.94, β is the maximum full width at half maximum (*FWHM*), and θ is the peak position. The diffraction peak at (101) is considered with the maximum intensity. Table 2 compares the estimated sizes obtained from the three methods described above. Note that the Scherrer equation is limited in making accurate estimations of the crystallite size because it does not account for the strain present in the lattice because of imperfections or defects. Therefore, other methods are necessary to estimate the QD size accurately; one of these methods involves the use of the Williamson-Hall (W–H) plot. Here, the strain is assumed to be uniform in all crystallographic directions; this assumption considers the isotropic nature of the crystals wherein all of the material properties are independent of the direction along which they are measured.

FESEM images of the samples are clearly shown inFigure2, which reveals the presence of high-density ZnO QDs. The particle sizes (from ~10 nm to ~22 nm) estimated from the FESEM images conform to those

determined from the XRD results. The integrated volume and sizes of the QDs increase during annealing as some of the ZnO atoms move from the wetting layer into the QDs. The dot distributions coarsen during annealing over a portion of the temperature range. Thus, the observed coarsening represents the size increment toward the lowest-energy configuration of the system consistent with increasing temperature. The Ostwald ripening process is responsible for the coarsening mechanism. Consequently, the free energy of the dots decreases monotonically with increasing QD size.

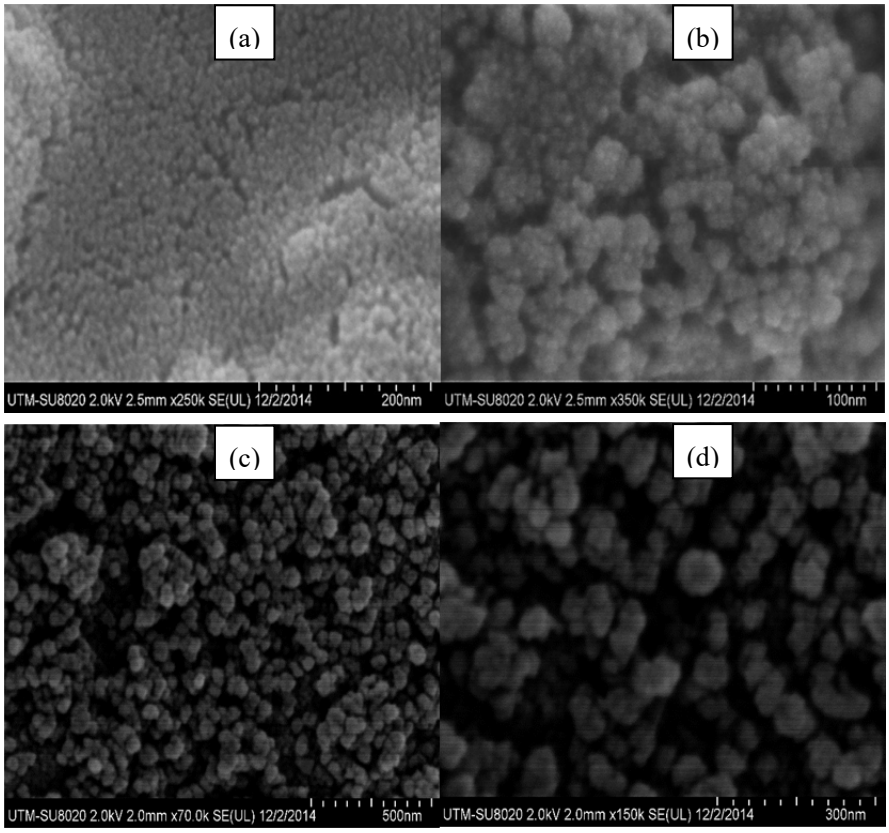

Figure 2. FESEM images of the ZnO QDs at different annealing temperature 425 (a), 450 (b), 475 (c) and 500 °C (d)

The term $\beta \cos\theta$ is plotted with respect to $4 \cdot \sin\theta$ to determine the preferred orientation peaks of ZnO QDs with respect to the wurtzite hexagonal phase. The slope and y-intersect of the fitted line respectively represent the strain and particle size of the QDs. The plots display a positive strain for the ZnO QDs, which could be attributed to the lattice expansion observed during calculation of the lattice parameters. The results of W–H analysis of the ZnO QDs are shown in Figure 3. It is clearly seen from the table that by increasing the annealing temperature, the strain is reduced due to inter-diffusion of Si substrate into ZnO and formation of ZnO-Si alloy.

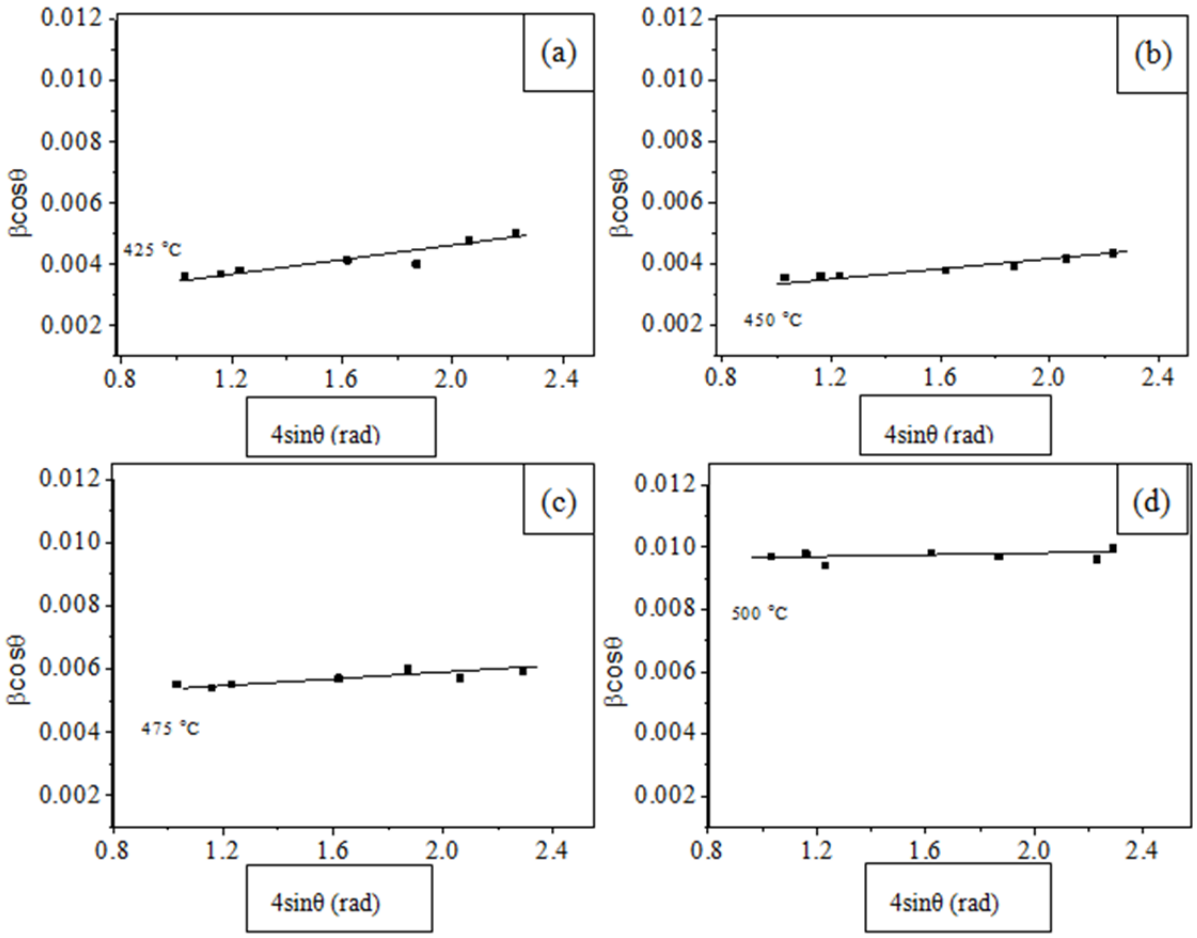

Figure 3. The W-H analysis of ZnO QDs at different annealing temperature 425 (a), 450 (b), 475 (c) and 500 °C (d)

The strain may be extracted from the slope and the crystalline size may be extracted from the y-intercept of the line obtained by fitting the data.

The EDX spectra of the samples are illustrated in Figure 4. All of characteristic peaks match the unique elements of Zn and O well. The peak of O decreases with increasing annealing temperature because of Zn diffusion into the Si substrate, which creates more oxygen vacancies.

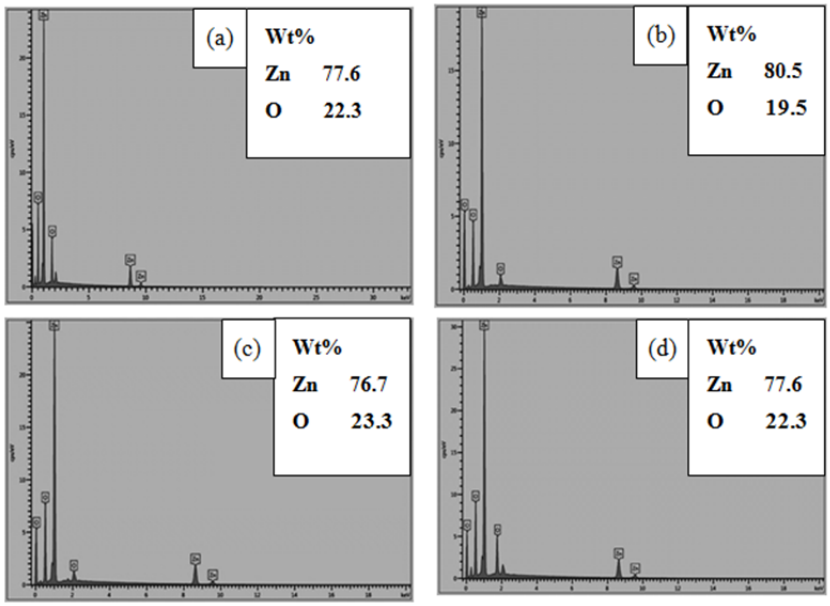

Figure 4. EDX spectra of ZnO QDs at different annealing temperature 425 (a), 450 (b), 475(c) and 500 °C (d)

The room-temperature PL spectra of the QDs are measured to investigate their optical properties as well as that of the resultant film. Figure 5 show that the PL spectra of the ZnO QDs show some dependence on the annealing temperature over the range of 425–500 °C. The peak at 368 nm (3.37eV) is characteristic of neutral-donor-bound-exciton (D0X) emission (Zhanget al., 2004; Ashrafi et al., 2004).The appearance of a weak shoulder at ~2.89 eV (violet region) is attributed to radiative recombination from intrinsic defects in the ZnO dots. Quantum confinement effects are not observed in the PL spectra because the size of the QDs is considerably larger than the exciton Bohr radius of ZnO (2.34 nm)(Wang et al., 2011).

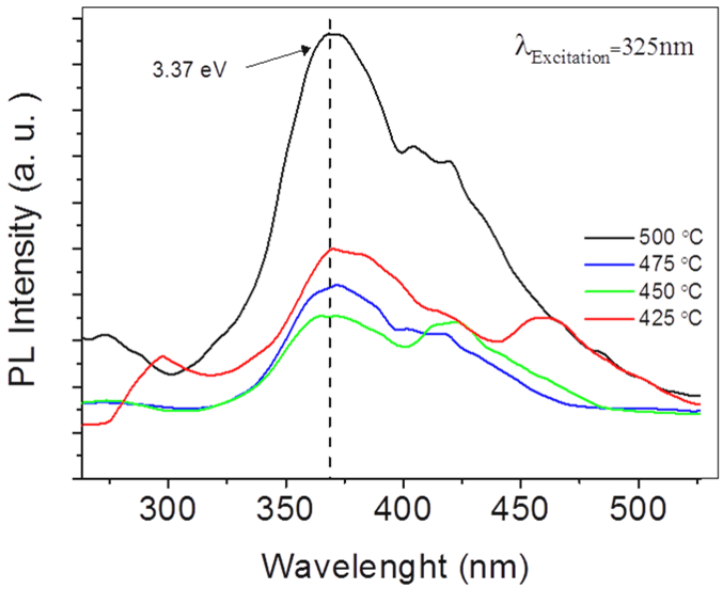

Figure 5. Room temperature PL spectra of ZnO QDs at different annealing temperature

4. Conclusion

Nearly spherical shaped high density ZnO QDs /Si are synthesized via facile yet accurate sol-gel method and spin coating. The influence of annealing temperature on ZnO QDs is found to alter the crystalline structures via

defect mediated strain interactions and broadens the spectral width. This in turn modifies the lattice parameters and elastic constants of the single crystalline QDs phase. The QDs size estimation through different methods reveals consistent measurements. The XRD measurement exhibits the wurtzite structure. The observed broadening is analyzed using the Scherrer formula and the W-H plot. The crystallite size is increased with increasing of annealing temperature. The FESEM image manifested presence of ZnO QDs with mean dot size between ~10 to 22 nm. EDX spectra confirm the inter-diffusion of ZnO into substrate layer, resulted to reduce the strain. The appearance of UV and blue-violet band in the room temperature PL spectra are ascribed to the electron–hole recombination from excited state to the ground-state and intrinsic defects belonging to ZnO QDs respectively. Quantum confinement effect is not observed as the QDs sizes are significantly larger than exciton Bohr radius for ZnO.

References

Ashrafi, A. B. M. A., Binh, N. T., Zhang, B. P., & Segawa, Y. (2004). Temperature-dependent photoluminescence of ZnO layers grown on 6H-SiC substrates. *J. Appl. Phys., 95*, 7738. http://dx.doi.org/10.1063/1.1649451

Barret, C. S., & Massalski, T. B. (1980). *Structure of Metals Pergamon*. Press Oxford. http://dx.doi.org/10.1002/crat.19810160904

Cullity, B. D. (1956). *Elements of X-ray Diffraction*. Addison-Wesley Publishing Company Inc.

Ergin, B., Ketenci, E., & Atay, F. (2009). Characterization of ZnO films obtained by ultrasonic spray pyrolysis technique.*J. Hydrogen Energy*. http://dx.doi.org/10.1016/j.ijhydene.2008.09.108

Ghosh, R., Basak, D., & Fujihara, S. (2004). Effect of substrate-induced strain on the structural, electrical, and optical properties of polycrystalline ZnO thin films. *J. Appl. Phys.*, 2689. http://dx.doi.org/10.1063/1.1769598

Gondal, M. A., Drmosh, Q. A., Yamani, Z. H., & Saleh, T. A. (2009). Synthesis of ZnO2 nanoparticles by laser ablation in liquid and their annealing transformation into ZnO nanoparticles. *Applied surface science*, 298-304. http://dx.doi.org/10.1016/j.apsusc.2009.08.019

Kamalianfar, A., Halim, S. A., & Zak, A. K. (2014). Synthesis of ZnO/Cu micro and nanostructures via a vapor phase transport method using different tube systems. *Ceramics International*, 3193–3198.

Liu, C., Liu, Z., Li, J., Li, Y., Han, J., Wang, Y., … Ya, J. (2013). Cu-doping ZnO/ZnS nanorods serve as the photoanode to enhance photocurrent and conversion efficiency. *Microelectronic Engineering, 103*, 12-16. http://dx.doi.org/10.1016/j.mee.2012.09.006

Mandal, S., Goswami, M. L. N., Das, K., Dhar, A., & Ray, S. K. (2008). Temperature dependent photoluminescence characteristics of nanocrystalline ZnO films grown by sol–gel technique. *Thin Solid Films*, 8702-8706. http://dx.doi.org/10.1016/j.tsf.2008.05.016

Rad, M. S., Kompany, A., Zak, A. K., Javidi, M., & Mortazavi, S. M. (2013). Microleakage and antibacterial properties of ZnO and ZnO:Ag nanopowders prepared via a sol–gel method for endodontic sealer application. *Journal of nanoparticle research*. http://dx.doi.org/10.1007/s11051-013-1925-6

Ramgir, N. S., Hwang, Y. K., Mulla, I. S., & Chang, J. S. (2006). Effect of particle size and strain in nanocrystalline SnO2 according to doping concentration of ruthenium. *Solid State Sciences*, 359-362. http://dx.doi.org/10.1016/j.solidstatesciences.2006.02.008

Razali, R., Zak, A. K., Abd Majid, W. H., & Darroudi, M. (2011). Solvothermal synthesis of microsphere ZnO nanostructures in DEA media. *Ceramics international*, 3657–3663. http://dx.doi.org/10.1016/j.ceramint.2011.06.026

Shahzad, M. B., Yang, Q., Hong, L., & Xiandi, W. (2013). A study on the Al doping behavior with sol aging time and its effect on structural and optical properties of sol–gel prepared ZnO thin films. T*hin solid films,* 242–248. http://dx.doi.org/10.1016/j.tsf.2013.02.126

Tekmen, A., S, Köç, P, Tüzemen, S., Meral, K., & Onganer, Y. (2013). UV-visible detector and LED based n-ZnO/p-Si heterojunction formed by electrodeposition. *AIP Publishing. AIP Advances, 3*(3), 032125. http://dx.doi.org/10.1021/nl070111x

Thomas, D., Abraham, J., Sunil, C. V., Augustine, S., & Thomas, D. T. (2014).Thomas, Abraham, Sunil, Augustine, & Dennis Thomas.). *American Journal of Pharm. Research, 4*(03), 1612-1616.

Wang, N., Yang, Y., & Yang, G. (2011).Great blue-shift of luminescence of ZnO nanoparticle array constructed from ZnO quantum dots. *Nanoscale Research Letters*, 1-6.

Yakuphanoglu, F., Ilican, S., Caglar, M., & Caglar, Y. (2007). The determination of the optical band and optical constants of non-crystalline and crystalline ZnO thin films deposited by spray pyrolysis. *J. Optoelectron. Adv. Mater, 9*, 2180.

Yousefi, R., Jamali Sheini, F., & Zak, A. K. (2012). Effect of indium concentration on morphology and optical properties of In-doped ZnO nanostructures. *Chemical Vapor Deposition*, 6295-6301. http://dx.doi.org/10.1016/j.ceramint.2012.04.085

Yousefi, R., JamaliSheini, F., Sa'aedi, A., Zak, A. K., Cheraghizade, M., PilbanJahromi, S., & Huang, N. M. (2013). Influence of lead concentration on morphology and optical properties of Pb-doped ZnO nanowires. *Ceramics International*, 9115–9119. http://dx.doi.org/10.1016/j.ceramint

Yousefi, R., Muhammad, M. R., & Zak, A. K. (2010). Investigation of indium oxide as a self-catalyst in ZnO/ZnInO heterostructure nanowires growth. *Thin Solid Films*, 5971–5977. http://dx.doi.org/10.1016/j.tsf.2010.05.111

Yousefi, R., Zak, A. K., & JamaliSheini, F. (2013). The effect of group-I elements on the structural and optical properties of ZnO nanoparticles. *Ceramics International*, 1371–1377. http://dx.doi.org/10.1016/j.ceramint.2012.07.076

Zak, A. K., Majid, W. A., Abrishami, M. E., Yousefi, R., & Parvizi, R. (2012). Synthesis, Magnetic Properties and X-ray Analysis of Zn0.97X0.03O Nanoparticles (X = Mn, Ni, and Co) using Scherrer and Size-Strain Plot Methods. *Solid State Sciences*, 488-494.

Zak, A. K., Wang, H. Z., Yousefi, R., Golsheikh, A. M., & Ren, Z. F. (2013). Sonochemical synthesis of hierarchical ZnO nanostructures. *Ultrasonics Sonochemistry*, 395–400. http://dx.doi.org/10.1016/j.ultsonch.2012.07.001

Zak, A. K., Yousefi, R., Majid, W. A., & Muhamad, M. R. (2012). Facile Synthesis and X-ray Peak Broadening Studies of Zn1-xMgxO Nanopaiticles. *Ceramics International*, 2059-2064. http://dx.doi.org/10.1016/j.ceramint.2011.10.042

Zamiri, R. A., Zakaria, A., Jorfi, R., Zamiri, G., Mojdehi, M. S., Ahangar, H. A., & Zak, A. K. (2013). Laser assisted fabrication of ZnO/Ag and Zn/Au core/shell nanocomposites. *Applied Physics A*. http://dx.doi.org/10.1007/s00339-012-7517-y

Zhang, B. P., Binh, N. T., Wakatsuki, K., Segawa, Y., Yamada, Y., Usami, N., … Koinuma, H. (2004). Formation of highly aligned ZnO tubes on sapphire (0001) substrates. *J. Phys. Chem. B10830*, 10899-10902. http://dx.doi.org/10.1063/1.1753061

Zhang, Y., Lin, B., Fu, Z., Liu, C., & Han, W. (2006). Strong ultraviolet emission and rectifying behavior of nanocrystalline ZnO films. *Opt. Mater.*, *1*, 192–1196. http://dx.doi.org/10.1016/j.optmat.2005.08.016